

# Co-assembly of Peptide Amphiphiles and Lipids into Supramolecular Nanostructures Driven by Anion- $\pi$ Interactions

Zhilin Yu,<sup>†,○,□</sup> Aykut Erbas,<sup>‡,○</sup> Faifan Tantakitti,<sup>‡</sup> Liam C. Palmer,<sup>†,§</sup> Joshua A. Jackman,<sup>||,#</sup> Monica Olvera de la Cruz,<sup>\*,†,‡,∇</sup> Nam-Joon Cho,<sup>\*,||,#,⊗</sup> and Samuel I. Stupp<sup>\*,†,‡,§,¶,◇</sup>

<sup>†</sup>Department of Chemistry, Northwestern University, Evanston, Illinois 60208, United States

<sup>‡</sup>Department of Materials Science and Engineering, Northwestern University, Evanston, Illinois 60208, United States

<sup>§</sup>Simpson Querrey Institute for BioNanotechnology, Northwestern University, Chicago, Illinois 60611, United States

<sup>||</sup>School of Materials Science and Engineering, Nanyang Technological University, 639798 Singapore

<sup>#</sup>Centre for Biomimetic Sensor Science, Nanyang Technological University, 639798 Singapore

<sup>∇</sup>Department of Physics, Northwestern University, Evanston, Illinois 60208, United States

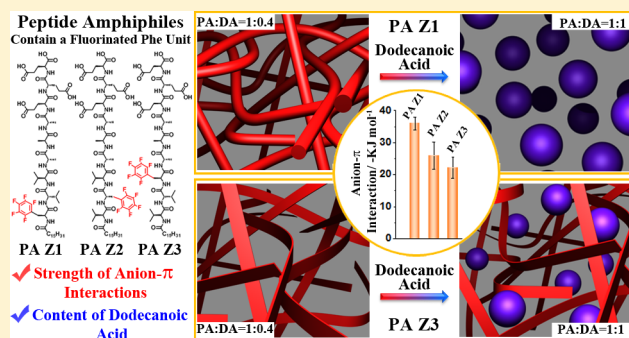
<sup>⊗</sup>School of Chemical and Biomedical Engineering, Nanyang Technological University, 639798 Singapore

<sup>¶</sup>Department of Medicine, Northwestern University, Chicago, Illinois 60611, United States

<sup>◇</sup>Department of Biomedical Engineering, Northwestern University, Evanston, Illinois 60208, United States

## Supporting Information

**ABSTRACT:** Co-assembly of binary systems driven by specific non-covalent interactions can greatly expand the structural and functional space of supramolecular nanostructures. We report here on the self-assembly of peptide amphiphiles and fatty acids driven primarily by anion- $\pi$  interactions. The peptide sequences investigated were functionalized with a perfluorinated phenylalanine residue to promote anion- $\pi$  interactions with carboxylate headgroups in fatty acids. These interactions were verified here by NMR and circular dichroism experiments as well as investigated using atomistic simulations. Positioning the aromatic units close to the N-terminus of the peptide backbone near the hydrophobic core of cylindrical nanofibers leads to strong anion- $\pi$  interactions between both components. With a low content of dodecanoic acid in this position, the cylindrical morphology is preserved. However, as the aromatic units are moved along the peptide backbone away from the hydrophobic core, the interactions with dodecanoic acid transform the cylindrical supramolecular morphology into ribbon-like structures. Increasing the ratio of dodecanoic acid to PA leads to either the formation of large vesicles in the binary systems where the anion- $\pi$  interactions are strong, or a heterogeneous mixture of assemblies when the peptide amphiphiles associate weakly with dodecanoic acid. Our findings reveal how co-assembly involving designed specific interactions can drastically change supramolecular morphology and even cross from nano to micro scales.



## INTRODUCTION

Supramolecular assemblies of binary systems have great potential in the search for functional systems. Examples include co-assembly of bioactive and nonbioactive molecules to tune the intensity of a response, or the co-assembly of a drug with its vehicle.<sup>1–5</sup> One of the design aspects of these systems is the use of specific interactions among the components of the binary biopolymers<sup>6,7</sup> or peptides,<sup>8–11</sup> or to use thermodynamically nonmiscible molecular segments in block copolymers or Janus dendrimers.<sup>12–14</sup> The literature contains a wide array of examples of self-assembling building blocks with structural features that favor non-covalent bonding among molecules, most commonly hydrogen bonding, metal–ligand interactions, and  $\pi$ -orbital overlaps.<sup>15–19</sup> The literature remains scarce on

other specific interactions, and co-assembly involving binary systems.

While traditional  $\pi$ -effects, including  $\pi$ , $\pi$ -stacking<sup>20</sup> and cation- $\pi$  interactions,<sup>21</sup> are relatively well understood in the context of molecular self-assembly, the interaction between negatively charged groups and electron deficient aromatic moieties, referred to as anion- $\pi$  interactions,<sup>22–24</sup> remains less investigated. Anion- $\pi$  interactions formed by a positive quadrupole on aromatic rings by electron withdrawing substituents were first reported in 2002,<sup>22</sup> and since have been explored by crystallography<sup>25</sup> and the molecular recognition of anions<sup>26</sup> or zwitterions.<sup>27</sup> However, despite

Received: February 28, 2017

Published: June 1, 2017

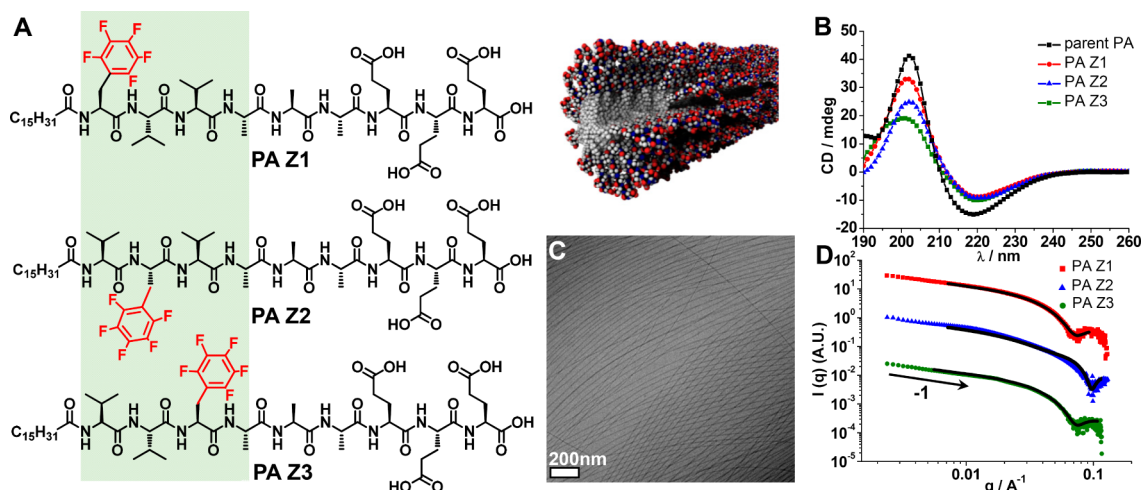


**Figure 1.** (A) Chemical structures of PA Z1, PA Z2, and PA Z3 containing perfluorophenylalanine (Z) at various positions. (B) Circular dichroism spectra of PA Z1, PA Z2, PA Z3, and the parent PA in water (50 μM) at 25 °C. (C) Representative cryo-TEM image of cylindrical fibers formed by PA Z1. (D) SAXS profiles of PA solutions plotting scattered intensity versus the scattering vector  $q$  (log–log plot) in water. Scattering intensities are offset vertically for clarity and the fitting curves for the scattering data are shown in black.

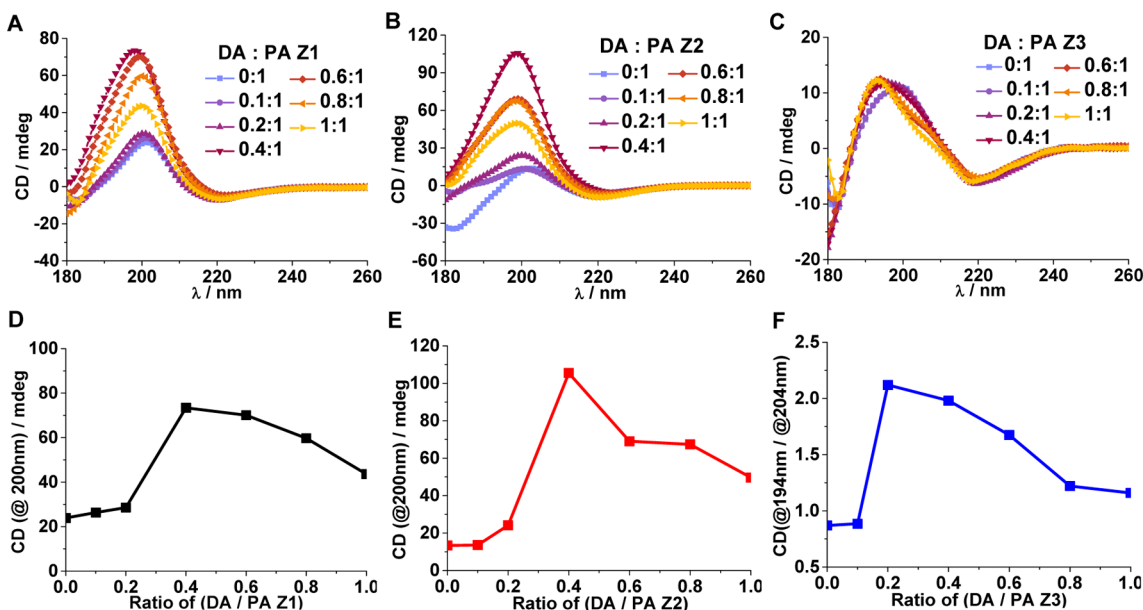


**Figure 2.** (A–C) CD spectra of mixed aqueous solutions of PA Z1 (A), PA Z2 (B), and PA Z3 (C) with dodecanoic acid [DA] aged for 2 h at 25 °C. (D,E) CD intensity at 200 nm as a function of DA/PA molar ratio for PA Z1 (D) and for PA Z2 (E). (F) Ratio of CD intensities at 194 and 204 nm for PA Z3 as a function of DA/PA molar ratio.

growing recognition of the multifaceted roles that anion– $\pi$  interactions play in biological systems<sup>28,29</sup> and their potential as design motifs in synthetic biology,<sup>30,31</sup> to the best of our knowledge their use in self-assembly of monomers into supramolecular nanostructures has not been reported. We report here on the binary self-assembly of amphiphiles into supramolecular nanostructures driven largely by anion– $\pi$  interactions. We investigate the morphology of these assemblies as a function of the strength of anion– $\pi$  interactions and their molecular composition.

We employed a peptide amphiphile and a fatty acid as the two components that should associate primarily driven by anion– $\pi$  interactions. Peptide amphiphiles (PAs) containing an amino acid sequence substituted by an alkyl chain can form nanostructures with a variety of morphologies in water, mostly depending on their primary structure.<sup>32–42</sup> Fatty acids are of

course well-known to assemble into a rich variety of supramolecular architectures driven by electrostatic interactions and hydrophobic effects.<sup>43,44</sup> We used dodecanoic acid as the second component due to its relatively high solubility in water. From a functional standpoint, dodecanoic acid was also of interest because of its known antibacterial activity often retained in nanoscale assemblies.<sup>45</sup> We incorporated one fluorinated phenylalanine residue (Z)<sup>46–50</sup> as the electron-deficient amino acid into the V<sub>3</sub>A<sub>3</sub>E<sub>3</sub> peptide sequence of a PA. The Z amino acid replaced one V residue in different positions, hence the nomenclature of PAs Z1, Z2, and Z3 (Figure 1A). We hypothesized that the 12-carbon alkyl tail of dodecanoic acid would bury itself in the hydrophobic core composed of palmitoyl tails within the supramolecular structures. In addition, varying the position of the Z residue would allow us to optimize the relative distance between the fluorinated aromatic groups

and carboxyl acid headgroups. This would in turn maximize anion- $\pi$  interactions between PA molecules and dodecanoic acid.

## RESULTS AND DISCUSSION

In an effort to establish how the position of the Z residue affects supramolecular morphology, we first characterized the self-assembly behavior of the PAs alone in water by circular dichroism (CD) spectroscopy, cryogenic transmission electron microscopy (cryo-TEM), and small-angle X-ray scattering (SAXS). Similar to the canonical PA that lacks the Z residue,<sup>51</sup> CD spectroscopic measurements showed that PA Z1, Z2, and Z3 all adopted predominantly  $\beta$ -sheet secondary structure in solution (Figure 1B), indicating that  $\beta$ -sheet hydrogen bonds can still be formed among amino acid sequences that contain a fluorinated aromatic unit. Compared to the parent PA, we found that at the same concentration either the incorporation of the Z residue into peptide backbones or moving the Z residue along peptide backbones away from the alkyl tail decreases the CD intensity of PAs. The decrease of the CD intensity is likely indicative of the reduction of the  $\beta$ -sheet composition in supramolecular nanostructures, potentially due to interference by the bulky Z residue in formation of hydrogen bonds. In terms of morphology, well-defined cylindrical nanofibers with a 7–10 nm diameter were formed by all three PAs in aqueous solution as observed by cryo-TEM (Figure 1C). The morphology of the PA assemblies was also confirmed by SAXS scattering experiments. The scattering signals showed an approximately  $-1$  slope in the low- $q$  region for all the PAs, supporting the cryo-TEM observation of cylindrical nanofibers as the dominant morphology (see Figure 1D). The diameter of the one-dimensional filaments was estimated to be approximately 8 nm, as determined by fitting the scattering curves to a core-shell cylinder model. Collectively, these results demonstrate that all the designed PAs form well-defined one-dimensional nanostructures in water in spite of the presence of the Z residue in the peptide sequence. The Z residue would be expected to contribute to steric interactions within the  $\beta$ -sheets in the internal structure of the supramolecular filaments but obviously does not disrupt the well-known self-assembly behavior of PA molecules.

We subsequently studied the binary co-assembly of the designed PAs and dodecanoic acid by CD spectroscopy. Solutions of PA Z1 or Z2 were mixed with dodecanoic acid and then aged for 2 h at room temperature. The resulting samples showed a substantial increase in CD intensity at 200 nm compared with that of PA solutions alone (Figure 2A,B), suggesting an enhancement of hydrogen bonding among monomers in  $\beta$ -sheets within the assemblies when a small amount of dodecanoic acid is incorporated.<sup>52,53</sup> The increase of the  $\beta$ -sheet CD signals could be attributed to reduction of electrostatic repulsion among PA molecules in the binary systems due to intercalation of dodecanoic acid molecules. The intensity of CD signals at 200 nm reached a maximum value after the addition of approximately 0.4 mol equiv of dodecanoic acid, and then gradually decreased with further addition (Figure 2D,E). These results indicate that the  $\beta$ -sheet hydrogen bonds are disrupted by associating the PAs Z1 and Z2 with a large fraction of dodecanoic acid. In marked contrast, mixing the solutions of PA Z3 with dodecanoic acid and aging for 2 h led to a blue shift for the positive peak across the entire titration process (Figure 2C). We therefore conclude that association of PA Z3 assemblies with dodecanoic acid alters the hydrogen

bonding of PA monomers in supramolecular assemblies. As a control experiment, the addition of dodecanoic acid to the parent PA without the Z residue yielded an initial increase in the CD intensity up to a value of 0.25 mol equiv of dodecanoic acid and the CD signals did not change with further addition of dodecanoic acid (Figure S5). The invariant CD spectral signature of the parent PA upon addition of greater fractions than 0.25 mol equiv of dodecanoic acid could be attributed to incomplete encapsulation of additional dodecanoic acid and excess of the lipid likely remains free in solution, potentially due to weak interactions with the parent PA molecules compared with those in binary systems involving PA Z1/Z2/Z3. This result suggests that the incorporation of the Z unit allows the PAs to strongly associate with dodecanoic acid molecules driven by anion- $\pi$  interactions, thus leading to co-assembly of both components.

To directly and qualitatively verify the anion- $\pi$  interaction between dodecanoic acid molecules and the PAs as well as monitor the location of dodecanoic acid molecules within the assemblies, we carried out <sup>19</sup>F NMR experiments on the PAs alone and also on the binary co-assemblies with dodecanoic acid. NMR has been a common technique used in previous work to probe anion- $\pi$  interactions in solution.<sup>54–56</sup> The *ortho*-, *meta*-, and *para*-fluorine atoms from the phenyl groups were clearly identified in the <sup>19</sup>F NMR spectra (Figure S7). Using the conditions that showed a maximum in the CD intensity, we found that simultaneously dissolving the PAs and dodecanoic acid in a molar ratio of 1:0.4 led to separation of the signals into two distinct resonances for both the *meta*- and *para*-fluorine atoms (Figure S7). In the cases of PA Z1 and PA Z2, the main peaks for the *meta*- and *para*-fluorine atoms exhibited down- and upfield shifts, respectively, while the minor peaks of *meta*- and *para*-fluorine of PA Z3 displayed down- and upfield shifts, respectively. The substantial separation and shift of the NMR signals of fluorine atoms are in principle attributed to the anion- $\pi$  interactions between the PAs and fatty acids.<sup>57</sup> It is important to note that although the PAs also contain three carboxylic acids in glutamic acid residues, the fluorine NMR signals on the PAs alone do not show any shift or separation, suggesting that anion- $\pi$  interactions are negligible in PA assemblies. Overall, the <sup>19</sup>F NMR results strongly indicate that the PAs and dodecanoic acid molecules are successfully co-assembled and associate via anion- $\pi$  interactions. In particular, positioning the Z residue closer to the N-terminus of the PAs results in greater separation and shift of the fluorine signals, indicating that the PAs interact with dodecanoic acid molecules via anion- $\pi$  interactions that decrease in strength in the following order, PA Z1 > PA Z2 > PA Z3. The different intensities of the anion- $\pi$  interaction revealed by <sup>19</sup>F NMR experiments also imply that dodecanoic acid molecules prefer to reside within the hydrophobic core of the PA assemblies. To confirm changes in the <sup>19</sup>F NMR signals induced by anion- $\pi$  interactions, one trifluoro-ethyl laurate (F-ethyl laurate) without the negatively charged headgroup was used to investigate the effect of its encapsulation on the fluorine signals in the <sup>19</sup>F NMR spectra. In the mixture of F-ethyl laurate and PA Z1, the fluorine signals did not show any shift or separation (Figure S8), indicating that encapsulation of small molecules into the PA assemblies does not give rise to the change of fluorine signals. These additional NMR experiments clearly demonstrate the occurrence of anion- $\pi$  interactions between the investigated PAs and dodecanoic acid.

We further quantified the interaction between the PAs and dodecanoic acid using isothermal titration calorimetry (ITC)<sup>58</sup> by recording the thermodynamic parameters obtained upon the addition of dodecanoic acid molecules to preformed PA assemblies. The thermodynamic parameters of the formation of the complexes containing PAs and dodecanoic acid are shown in Table 1 (Figure S9). Addition of dodecanoic acid into

**Table 1. Thermodynamic Parameters for the Complexes Formed between the PA Molecules and Dodecanoic Acid (DA) in Water at 25 °C**

	PA Z1 + DA	PA Z2 + DA	PA Z3 + DA
binding constant/ (mol/L) <sup>-1</sup>	$5.49 \times 10^4 \pm 5357$	$4.56 \times 10^4 \pm 1215$	$9.95 \times 10^3 \pm 252$
$\Delta H/\text{kJ mol}^{-1}$	$-38.12 \pm 1.22$	$-10.54 \pm 1.01$	$-15.23 \pm 4.52$
$\Delta S/\text{J mol}^{-1}$	$37.07 \pm 3.52$	$-29.04 \pm 2.43$	$-53.85 \pm 5.61$
$\Delta G/\text{kJ mol}^{-1}$	-49.19	-1.86	0.85

all three PA solutions resulted in a negative enthalpy change, suggesting the enhancement of  $\beta$ -sheet hydrogen bonds among PA monomers in their assemblies. Interestingly, only a positive entropy change was observed in the formation of the complex of PA Z1 and dodecanoic acid, possibly indicating the release of structured water molecules when these highly favorable interactions occur between PA Z1 and dodecanoic acid carboxylate groups.<sup>59</sup> ITC results confirm that the affinity between dodecanoic acid and the PAs is enhanced due to anion- $\pi$  interactions, the strength of which varies depending on the location of the Z residue within the PA structure.

Following our experimental observations of the strong association between the designed PAs and dodecanoic acid molecules, we investigated the morphology of the binary co-assemblies using conventional TEM, cryo-TEM, and SAXS. Dissolving in water at the same time PA Z1 or Z2 and dodecanoic acid in a molar ratio of 1:0.4 resulted in the

formation of cylindrical nanofibers as revealed by cryo-TEM, similar to the nanostructures formed by the PAs alone. In contrast, mixing PA Z3 with dodecanoic acid in a 1:0.4 molar ratio led to formation of ribbon-like flat nanostructures. This morphological difference between the co-assemblies involving PA Z3 and PA Z1 or Z2 is consistent with the variations of CD spectral changes upon addition of dodecanoic acid, which revealed a blue shift for PA Z3 and an increase in signal intensity for PA Z1 and PA Z2. While intercalation of fatty acids into the hydrophobic interior of the PA cylinders may expand the space between the palmitoyl tails of all three PAs within their corresponding assemblies, the location of the Z residue and fatty acids as well as the strength of non-covalent interactions within the assemblies all contribute to the differences in nanostructures observed with the different PA sequences. In the binary system of PA Z3 and dodecanoic acid, we hypothesize that the co-assembled lipids partially translocate toward the interior of the  $\beta$ -sheet region driven by anion- $\pi$  interactions, changing the packing geometry of hydrophilic and hydrophobic segments compared with that associated with supramolecular structures formed by PA Z3 alone. Thus, we propose this change causes a morphological transition from cylindrical fibers formed by PA Z3 alone to ribbon-like structures consistent with the theory proposed by Israelachvili et al.<sup>60</sup> formed by the binary system. However, in the systems consisting of PA Z1 or Z2 and dodecanoic acid, lipids prefer to localize in the hydrophobic core, thus maintaining the packing geometry associated with cylindrical fibers for the binary systems. We further increased the content of dodecanoic acid in the co-assemblies to a 1:1 molar ratio in order to study how the molecular composition of the structures influences their morphology. In contrast to the cylindrical fibers formed by PA Z1 and dodecanoic acid molecules in a 1:0.4 molar ratio, conventional TEM revealed that large vesicles were formed by PA Z1 and dodecanoic acid molecules in a 1:1 molar ratio. The geometrical transformation is potentially due to the disruption

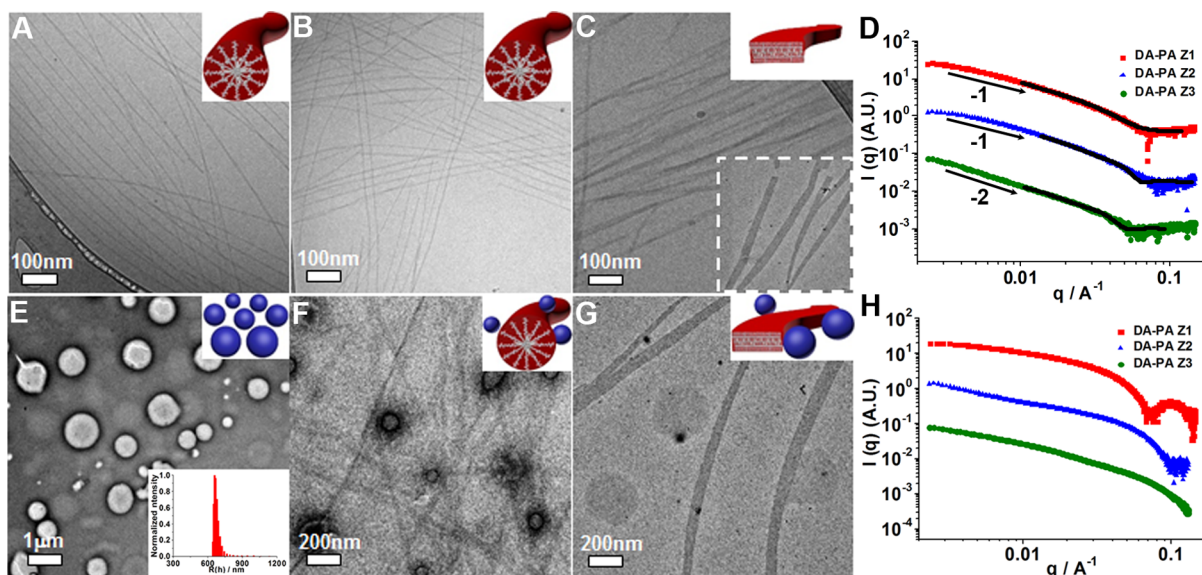


**Figure 3.** (A–C) Cryo-TEM images of mixtures of PA Z1, PA Z2, and PA Z3 with dodecanoic acid [DA] in a molar ratio of 1:0.4, and (E–G) conventional TEM images of mixtures in a 1:1 molar ratio without staining (schematic illustrations of the morphologies are shown in the insets). DLS data of the vesicles formed by PA Z1 and dodecanoic acid in 1:1 molar ratio are shown in the bottom inset in (E). (D,H) SAXS profiles of the DA–PA aqueous solutions in molar ratios of 1:0.4 (D) and 1:1 (H). The profiles plot scattered intensity versus the scattering vector  $q$  (log–log plot); scattering intensities are offset vertically for clarity, and the fitting curves for the scattering data are shown in black in (D).

of  $\beta$ -sheet hydrogen bonds among PA molecules caused by addition of a large fraction of dodecanoic acid, which dilutes the PA in binary systems. Dynamic light scattering (DLS) confirmed the presence of these large structures and was used to estimate a hydrodynamic radius of approximately 700 nm (Figure 3E, inset). On the other hand, mixing PA Z2 or Z3 with dodecanoic acid in a 1:1 molar ratio led to the formation of cylindrical filaments and vesicles or ribbons and vesicles, respectively, indicating formation of a heterogeneous collection of supramolecular co-assemblies. In the case of PA Z1, the morphological transition for the 1:1 binary co-assemblies is likely the result of a homogeneous geometry change in the complex formed by these two strongly interacting molecules. In contrast, the relatively weak interactions between the other PAs and fatty acids induce formation of binary co-assemblies containing varying amounts of fatty acids, and therefore a heterogeneous mixture of nanostructures.

We carried out atomistic molecular dynamics (MD) simulations<sup>61</sup> on the co-assemblies of PAs and dodecanoic acid using the Gromacs MD package<sup>62</sup> under the GROMOS force field.<sup>63</sup> After 300 ns simulations the secondary structure of peptide segments of PA molecules surrounded by water and sodium counterions reached a steady state and the cylindrical morphology of the PA assemblies was maintained (Figure 4A).

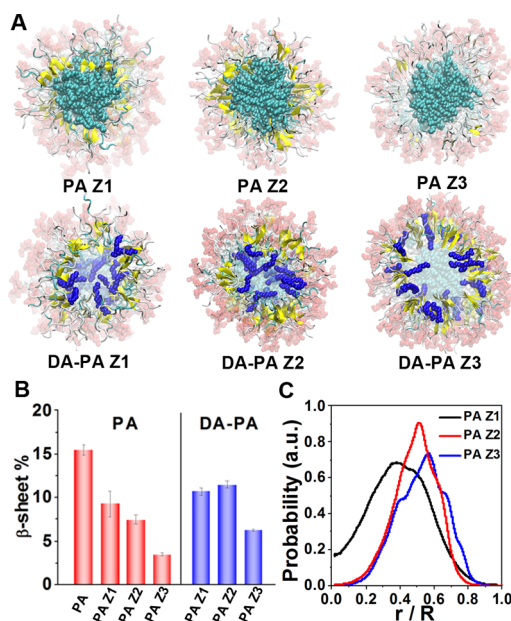


**Figure 4.** (A) Cross-sectional snapshots for PA cylindrical fibers without and with dodecanoic acid in a molar ratio of 1:0.2 after a 300 ns simulation (cyan: alkyl tails in PA molecules; blue: DA molecules; yellow:  $\beta$ -sheets strands). (B) Percentage of  $\beta$ -sheets in secondary structures of the PAs and their co-assemblies with dodecanoic acid in 1:0.2 molar ratio. (C) Cross-sectional distribution profile of dodecanoic acid molecules in the nanofibers as a function of normalized radius.

Compared to the parent PA, the simulation results show that incorporation of the Z residue gives rise to a decrease in  $\beta$ -sheet secondary structure within the assemblies (Figure 4B). Furthermore, positioning the Z residue closer to the C-terminus (from PA Z1 to Z2 and Z3) gradually lowers the content of  $\beta$ -sheet structures. The simulation results indicating a decrease of  $\beta$ -sheet structures induced by the incorporation of the Z unit or moving it along peptide backbones away from the

alkyl tail are consistent with experimental findings obtained from the CD intensity of the  $\beta$ -sheets formed by the various PAs. The  $\beta$ -sheet composition was estimated by MD simulations as 9.3%, 7.4%, and 3.5% for PAs Z1, Z2, and Z3, respectively. These results indicate that the bulky Z residue constrains formation of  $\beta$ -sheets potentially due to steric hindrance, which interferes with coupling between hydrogen bond donors and acceptors, particularly when the Z residue is located in the interior of the  $\beta$ -sheet region in the case of PA Z3.

MD simulations on the PA and dodecanoic acid binary systems were carried out under the same condition for the PAs alone. In 300 ns simulation we observed unstable nanofibers in binary co-assemblies of PA Z3 and dodecanoic acid in the 1:0.4 molar ratio (Figure S14), a finding which is consistent with the morphological transitions from cylindrical fibers formed by PA Z3 alone to flat ribbons formed by the binary system in a 1:0.4 molar ratio as observed in TEM experiments. Hence, in our simulations we investigated initial structures consisting of each PA and dodecanoic acid in a 1:0.2 molar ratio. The dodecanoic acid molecules are localized either randomly or regularly within the initial structures to maximize the reliability of the simulations (Figure S10B,C). After relaxation for at least 200 ns, the initial cylindrical morphology was maintained and the dodecanoic acid molecules reorganized within the fibers (Figure 4A). This suggests that co-assembly of PAs and dodecanoic acid in a 1:0.2 molar ratio leads to the formation of stable, well-defined cylindrical nanofibers.  $\beta$ -Sheet content in the binary complexes increases for all the three PAs compared to neat PA assemblies (Figure 4B). This result is consistent with the experimental observation in CD spectra, which suggest that encapsulation of dodecanoic acid molecules enables the optimal formation of  $\beta$ -sheet hydrogen bonds within the assemblies. This could be potentially attributed to the decrease of electrostatic repulsion among PA molecules due to their dilution in the binary systems upon addition of dodecanoic acid. In a more detailed evaluation, we profiled the cross-sectional radial distribution of dodecanoic acid molecules within the stable cylindrical fibers. Our simulations revealed that all of the added dodecanoic acid molecules were confined within the PA assemblies and the radial distribution of dodecanoic acid strongly depends on the position of the Z residue within the PA structures (Figure 4C). These results are consistent with the <sup>19</sup>F NMR studies, which reveal that dodecanoic acid molecules prefer to reside within the hydrophobic core of the supramolecular structures based on changes of the fluorine NMR signals. In the case of PA Z1, dodecanoic acid molecules are primarily buried in the hydrophobic core (Figure 4C, black curve), whereas in the cylindrical fibers formed by PA Z2 or Z3, dodecanoic acid molecules translocate outward relative to the periphery of the fibers. The distribution of the co-assembled dodecanoic acid molecules correlates with the location of the pentafluorobenzene moiety within the nanofibers (Figure 4C), indicating that the majority of dodecanoic acid molecules are localized around the Z residue. MD simulations strongly imply that anion- $\pi$  interactions between the PAs and dodecanoic acid play a critical role in their association, and thus control the location of fatty acids within the co-assemblies.

MD simulations also allow us to further estimate the strength of the  $\pi$ , $\pi$ -stacking and anion- $\pi$  interactions within the co-assemblies by evaluating the short-range electrostatic and steric interaction energies per PA monomer. The  $\pi$ , $\pi$ -stacking

interaction energy present in the assemblies formed by PAs alone is nearly identical and determined to be approximately  $-105 \text{ kJ mol}^{-1}$  (Figure 5A), suggesting that the relative

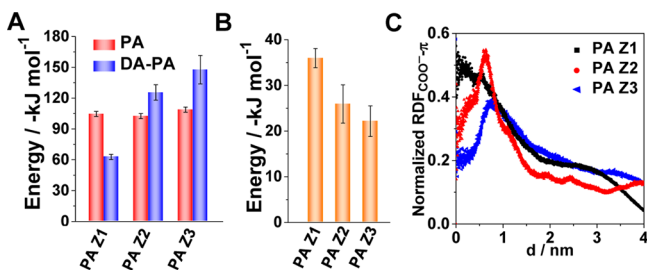


**Figure 5.** (A) Strength of  $\pi,\pi$ -stacking interactions estimated from simulations among aromatic groups in PA molecules in the absence and presence of dodecanoic acid molecules and (B) the anion- $\pi$  interactions between the PAs and dodecanoic acid molecules (PA:DA = 1:0.2). (C) Normalized radial distribution function (RDF) of the distance between the polar carboxylic acid functional group of dodecanoic acid molecules and the center of mass of pentafluorobenzene rings within the nanofibers (PA:DA = 1:0.2).

distance and orientation of the phenyl groups is independent of their location within the PA structures. However, co-assembling dodecanoic acid with the PA molecules results in variations of the strength of  $\pi,\pi$ -stacking depending on the position of the Z unit within the peptide backbone. The strength of  $\pi,\pi$ -stacking interactions among PA monomers was calculated to be  $-63$ ,  $-125$ , and  $-148 \text{ kJ mol}^{-1}$  for the binary systems containing PA Z1, Z2, and Z3, respectively. These results indicate that  $\pi,\pi$ -stacking interactions are retained in binary systems and contribute to the co-assembly of both molecules. On the other hand the co-assembled dodecanoic acid molecules alter the relative distance and orientation of the aromatic units within the assemblies due to their strong association with the PA molecules based primarily on anion- $\pi$  interactions. The relatively weak  $\pi,\pi$ -stacking interactions among PA Z1 monomers allow for the strong association between the PA and dodecanoic acid molecules in the binary system. The largest increase in  $\pi,\pi$ -stacking interactions induced by co-assembly with dodecanoic acid molecules occurs in PA Z3 and we hypothesize that this contributes to the morphological transition from the cylindrical fibers formed by PA Z3 alone to the ribbons formed by the PA-dodecanoic acid complexes, as revealed by TEM and SAXS experiments discussed above. Generally the simulation results support the concept that supramolecular morphology of the co-assemblies is directly affected by the strength of non-covalent interactions among components.

Based on the atomistic simulations, the anion- $\pi$  interaction energy between the Z residue and the carboxylic acid unit in dodecanoic acid molecules decreases from PA Z1 to PA Z2 and PA Z3 (Figure 5B). This result from simulations strongly suggests that PA molecules containing the Z unit closer to the N-terminus of peptide backbones exhibit the strongest anion- $\pi$  interactions with dodecanoic acid molecules. This is possibly due to the preferential localization of dodecanoic acid molecules in the hydrophobic core of the co-assemblies, thus leading to a short distance between the electron deficient aromatic units and carboxylic acids that promote strong anion- $\pi$  interactions. Therefore, we profiled the radial distribution function (RDF) of the distance between the polar carboxylic acid functional group of dodecanoic acid

molecules and the mass center of the pentafluorobenzene rings within the assemblies (Figure 5C). In the case of PA Z1, the charged head of dodecanoic acid molecules are predominantly localized within  $0.4 \text{ nm}$  of the aromatic units, a distance which places them in close proximity and favors the anion- $\pi$  interaction. However, the primary distance between the carboxylic acid of dodecanoic acid and the center of mass of the pentafluorobenzene ring within the PA Z2 and Z3 assemblies increases to  $0.6\text{--}0.7 \text{ nm}$ , a distance that is typically associated with lone pair- $\pi$  interactions.<sup>64</sup> This indicates that the main driving force for the association of PA Z2 or Z3 with dodecanoic acid molecules is linked to lone pair- $\pi$  interactions between the charged head of dodecanoic acid and the fluorinated phenyl groups and additional anion- $\pi$  interactions. Overall, our simulation results clearly demonstrate that the anion- $\pi$  interaction between PA and dodecanoic acid molecules determines the location of the encapsulated dodecanoic acid molecules within the co-assemblies.

## CONCLUSION

We have designed and synthesized three peptide amphiphiles containing one pentafluorophenyl alanine at different positions in the peptide backbones. Incorporation of the fluorinated phenyl groups that serve as electro-deficient units promotes anion- $\pi$  interactions between peptide amphiphiles and fatty acids. Both experimental and computational results confirm that localizing the fluorinated aromatic unit close to the N-terminus of the peptide backbone allows for strong anion- $\pi$  interactions in the binary systems, due to the preferential localization of fatty acids in the hydrophobic core of the co-assemblies. With such localized fatty acids, the binary systems co-assemble into cylindrical fibers, consistent with the morphology of the assemblies formed by peptide amphiphiles alone. However, positioning the aromatic unit in the interior of  $\beta$ -sheets promotes translocation of fatty acid molecules toward the hydrophilic region of binary assemblies, leading to a morphological transition from cylindrical fibers formed by the PA molecules alone to ribbon-like structures formed by the binary system. We also discovered that the strong association between PA and fatty acid molecules allows the binary systems with a large content of fatty acids to form uniform structures, while weak interactions give rise to a heterogeneous collection of assemblies.

## ASSOCIATED CONTENT

### Supporting Information

The Supporting Information is available free of charge on the ACS Publications website at DOI: 10.1021/jacs.7b02058.

Synthesis and purification of the PAs, characterizations, and atomistic MD simulations, including Figures S1–S14 (PDF)

## AUTHOR INFORMATION

### Corresponding Authors

\*m-olvera@northwestern.edu

\*njcho@ntu.edu.sg

\*s-stupp@northwestern.edu

### ORCID

Liam C. Palmer: 0000-0003-0804-1168

Nam-Joon Cho: 0000-0002-8692-8955

Samuel I. Stupp: 0000-0002-5491-7442

**Present Address**

□MOE Key Laboratory of Functional Polymer Materials, Institute of Polymer Chemistry, College of Chemistry, Nankai University, Tianjin 300071, China

**Author Contributions**

○Z.Y. and A.E. contributed equally to this work.

**Notes**

The authors declare no competing financial interest.

**ACKNOWLEDGMENTS**

This work was primarily supported by the Nanyang Technological University-Northwestern Institute of Nanomedicine (NNIN). CD and TEM experiments were supported by the U.S. National Science Foundation (NSF) under Award No. DMR 1508731. The simulation work was supported by the U.S. Department of Energy (DOE), Office of Science, Office of Basic Energy Sciences, under Award No. DE-FG02-08ER46539. SAXS experiments were performed at the DuPont–Northwestern–Dow Collaborative Access Team (DND-CAT) located at Sector 5 of the Advanced Photon Source (APS). DND-CAT is supported by E. I. DuPont de Nemours and Co., The Dow Chemical Company, and Northwestern University. This research used resources of APS, a U.S. DOE Office of Science User Facility operated for the DOE Office of Science by Argonne National Laboratory under Contract No. DE-AC02-06CH11357. This work made use of TEM, SEM, and AFM in the Electron Probe Instrumentation Center facilities of the Northwestern University Atomic and Nanoscale Characterization Experimental Center, which has received support from the Soft and Hybrid Nanotechnology Experimental (SHyNE) Resource (NSF ECCS-1542205); the MRSEC program (NSF DMR-1121262) at the Materials Research Center; the International Institute for Nanotechnology (IIN); the Keck Foundation; and the State of Illinois, through the IIN. Cryo-TEM was performed at the Northwestern University Biological Imaging Facility generously supported by the NU Office for Research. Peptide purification was performed in the Peptide Synthesis Core Facility of the Simpson Querrey Institute at Northwestern University. The U.S. Army Research Office, the U.S. Army Medical Research and Materiel Command, and Northwestern University provided funding to develop this facility. We are also grateful to the Keck Biophysics Facility for instrument use. A.E. thanks L. Martinez for the discussion on the PACKMOL code.

**REFERENCES**

- (1) Webber, M. J.; Appel, E. A.; Meijer, E. W.; Langer, R. *Nat. Mater.* **2016**, *15*, 13–26.
- (2) Silva, G. A.; Czeisler, C.; Niece, K. L.; Beniash, E.; Harrington, D. A.; Kessler, J. A.; Stupp, S. I. *Science* **2004**, *303*, 1352.
- (3) Dankers, P. Y. W.; Harmsen, M. C.; Brouwer, L. A.; Van Luyn, M. J. A.; Meijer, E. W. *Nat. Mater.* **2005**, *4*, 568–574.
- (4) Soukasene, S.; Toft, D. J.; Moyer, T. J.; Lu, H.; Lee, H.-K.; Standley, S. M.; Cryns, V. L.; Stupp, S. I. *ACS Nano* **2011**, *5*, 9113–9121.
- (5) Anraku, Y.; Kishimura, A.; Kamiya, M.; Tanaka, S.; Nomoto, T.; Toh, K.; Matsumoto, Y.; Fukushima, S.; Sueyoshi, D.; Kano, M. R.; Urano, Y.; Nishiyama, N.; Kataoka, K. *Angew. Chem., Int. Ed.* **2016**, *55*, 560–565.
- (6) Ringle, P.; Schulz, G. E. *Science* **2003**, *302*, 106–109.
- (7) Davis, M. E.; Zuckerman, J. E.; Choi, C. H. J.; Seligson, D.; Tolcher, A.; Alabi, C. A.; Yen, Y.; Heidel, J. D.; Ribas, A. *Nature* **2010**, *464*, 1067–1070.

- (8) Behanna, H. A.; Donners, J. J. J. M.; Gordon, A. C.; Stupp, S. I. *J. Am. Chem. Soc.* **2005**, *127*, 1193–1200.
- (9) Swanekamp, R. J.; DiMaio, J. T. M.; Bowerman, C. J.; Nilsson, B. L. *J. Am. Chem. Soc.* **2012**, *134*, 5556–5559.
- (10) Li, S.; Mehta, A. K.; Sidorov, A. N.; Orlando, T. M.; Jiang, Z.; Anthony, N. R.; Lynn, D. G. *J. Am. Chem. Soc.* **2016**, *138*, 3579–3586.
- (11) Wang, Z.; Zhang, F.; Wang, Z.; Liu, Y.; Fu, X.; Jin, A.; Yung, B. C.; Chen, W.; Fan, J.; Yang, X.; Niu, G.; Chen, X. *J. Am. Chem. Soc.* **2016**, *138*, 15027–15034.
- (12) Discher, D. E.; Eisenberg, A. *Science* **2002**, *297*, 967–973.
- (13) Gu, F.; Zhang, L.; Teply, B. A.; Mann, N.; Wang, A.; Radovic-Moreno, A. F.; Langer, R.; Farokhzad, O. C. *Proc. Natl. Acad. Sci. U. S. A.* **2008**, *105*, 2586–2591.
- (14) Percec, V.; Wilson, D. A.; Leowanawat, P.; Wilson, C. J.; Hughes, A. D.; Kaucher, M. S.; Hammer, D. A.; Levine, D. H.; Kim, A. J.; Bates, F. S.; Davis, K. P.; Lodge, T. P.; Klein, M. L.; DeVane, R. H.; Aqad, E.; Rosen, B. M.; Argintaru, A. O.; Sienkowska, M. J.; Rissanen, K.; Nummelin, S.; Ropponen, J. *Science* **2010**, *328*, 1009–1014.
- (15) Huang, Y.; Chiang, C.-Y.; Lee, S. K.; Gao, Y.; Hu, E. L.; Yoreo, J. D.; Belcher, A. M. *Nano Lett.* **2005**, *5*, 1429–1434.
- (16) Cui, H.; Webber, M. J.; Stupp, S. I. *Biopolymers* **2010**, *94*, 1–18.
- (17) Hobza, P.; Řezáč, J. *Chem. Rev.* **2016**, *116*, 4911–4912.
- (18) Cook, T. R.; Stang, P. J. *Chem. Rev.* **2015**, *115*, 7001–7045.
- (19) Würthner, F.; Saha-Möller, C. R.; Fimmel, B.; Ogi, S.; Leowanawat, P.; Schmidt, D. *Chem. Rev.* **2016**, *116*, 962–1052.
- (20) Meyer, E. A.; Castellano, R. K.; Diederich, F. *Angew. Chem., Int. Ed.* **2003**, *42*, 1210–1250.
- (21) Ma, J. C.; Dougherty, D. A. *Chem. Rev.* **1997**, *97*, 1303–1324.
- (22) Quiñero, D.; Garau, C.; Rotger, C.; Frontera, A.; Ballester, P.; Costa, A.; Deyà, P. M. *Angew. Chem., Int. Ed.* **2002**, *41*, 3389–3392.
- (23) Schottel, B. L.; Chifotides, H. T.; Dunbar, K. R. *Chem. Soc. Rev.* **2008**, *37*, 68–83.
- (24) Frontera, A.; Gamez, P.; Mascal, M.; Mooibroek, T. J.; Reedijk, J. *Angew. Chem., Int. Ed.* **2011**, *50*, 9564–9583.
- (25) de Hoog, P.; Gamez, P.; Mutikainen, I.; Turpeinen, U.; Reedijk, J. *Angew. Chem., Int. Ed.* **2004**, *43*, 5815–5817.
- (26) Dawson, R. E.; Hennig, A.; Weimann, D. P.; Emery, D.; Ravikumar, V.; Montenegro, J.; Takeuchi, T.; Gabutti, S.; Mayor, M.; Mareda, J.; Schalley, C. A.; Matile, S. *Nat. Chem.* **2010**, *2*, 533–538.
- (27) Perraud, O.; Robert, V.; Gornitzka, H.; Martinez, A.; Dutasta, J. P. *Angew. Chem., Int. Ed.* **2012**, *51*, 504–508.
- (28) Zhao, Y.; Cotellet, Y.; Sakai, N.; Matile, S. *J. Am. Chem. Soc.* **2016**, *138*, 4270–4277.
- (29) Giese, M.; Albrecht, M.; Rissanen, K. *Chem. Commun.* **2016**, *52*, 1778–1795.
- (30) Cotellet, Y.; Lebrun, V.; Sakai, N.; Ward, T. R.; Matile, S. *ACS Cent. Sci.* **2016**, *2*, 388–393.
- (31) Lucas, X.; Bauza, A.; Frontera, A.; Quinero, D. *Chem. Sci.* **2016**, *7*, 1038–1050.
- (32) Lowik, D. W. P. M.; van Hest, J. C. M. *Chem. Soc. Rev.* **2004**, *33*, 234–245.
- (33) Dehsorkhi, A.; Castelletto, V.; Hamley, I. W. *J. Pept. Sci.* **2014**, *20*, 453–467.
- (34) Yu, Y.-C.; Berndt, P.; Tirrell, M.; Fields, G. B. *J. Am. Chem. Soc.* **1996**, *118*, 12515–12520.
- (35) Hartgerink, J. D.; Beniash, E.; Stupp, S. I. *Science* **2001**, *294*, 1684–1688.
- (36) Vauthey, S.; Santoso, S.; Gong, H.; Watson, N.; Zhang, S. *Proc. Natl. Acad. Sci. U. S. A.* **2002**, *99*, 5355–5360.
- (37) Pashuck, E. T.; Stupp, S. I. *J. Am. Chem. Soc.* **2010**, *132*, 8819–8821.
- (38) Ghosh, A.; Haverick, M.; Stump, K.; Yang, X.; Tweedle, M. F.; Goldberger, J. E. *J. Am. Chem. Soc.* **2012**, *134*, 3647–3650.
- (39) Moyer, T. J.; Cui, H.; Stupp, S. I. *J. Phys. Chem. B* **2013**, *117*, 4604–4610.
- (40) Cui, H.; Cheatham, A. G.; Pashuck, E. T.; Stupp, S. I. *J. Am. Chem. Soc.* **2014**, *136*, 12461–12468.
- (41) Jin, H.-E.; Jang, J.; Chung, J.; Lee, H. J.; Wang, E.; Lee, S.-W.; Chung, W.-J. *Nano Lett.* **2015**, *15*, 7138–7145.

- (42) Chen, Y.; Gan, H. X.; Tong, Y. W. *Macromolecules* **2015**, *48*, 2647–2653.
- (43) Douliez, J.-P.; Gaillard, C. *New J. Chem.* **2014**, *38*, 5142–5148.
- (44) Fameau, A.-L.; Zemb, T. *Adv. Colloid Interface Sci.* **2014**, *207*, 43–64.
- (45) Jackman, J.; Yoon, B.; Li, D.; Cho, N.-J. *Molecules* **2016**, *21*, 305.
- (46) Pace, C. J.; Gao, J. *Acc. Chem. Res.* **2013**, *46*, 907–915.
- (47) Cejas, M. A.; Kinney, W. A.; Chen, C.; Leo, G. C.; Tounge, B. A.; Vinter, J. G.; Joshi, P. P.; Maryanoff, B. E. *J. Am. Chem. Soc.* **2007**, *129*, 2202–2203.
- (48) Cejas, M. A.; Kinney, W. A.; Chen, C.; Vinter, J. G.; Almond, H. R.; Balss, K. M.; Maryanoff, C. A.; Schmidt, U.; Breslav, M.; Mahan, A.; Lacy, E.; Maryanoff, B. E. *Proc. Natl. Acad. Sci. U. S. A.* **2008**, *105*, 8513–8518.
- (49) Ryan, D. M.; Anderson, S. B.; Senguen, F. T.; Youngman, R. E.; Nilsson, B. L. *Soft Matter* **2010**, *6*, 475–479.
- (50) Ryan, D. M.; Doran, T. M.; Nilsson, B. L. *Chem. Commun.* **2011**, *47*, 475–477.
- (51) Pashuck, E. T.; Cui, H.; Stupp, S. I. *J. Am. Chem. Soc.* **2010**, *132*, 6041–6046.
- (52) Hong, D.-P.; Hoshino, M.; Kuboi, R.; Goto, Y. *J. Am. Chem. Soc.* **1999**, *121*, 8427–8433.
- (53) Gursky, O.; Aleshkov, S. *Biochim. Biophys. Acta, Protein Struct. Mol. Enzymol.* **2000**, *1476*, 93–102.
- (54) Ballester, P. *Acc. Chem. Res.* **2013**, *46*, 874–884.
- (55) Guha, S.; Saha, S. *J. Am. Chem. Soc.* **2010**, *132*, 17674–17677.
- (56) Muller, M.; Albrecht, M.; Sackmann, J.; Hoffmann, A.; Dierkes, F.; Valkonen, A.; Rissanen, K. *Dalton Trans.* **2010**, *39*, 11329–11334.
- (57) Giese, M.; Albrecht, M.; Repenko, T.; Sackmann, J.; Valkonen, A.; Rissanen, K. *Eur. J. Org. Chem.* **2014**, *2014*, 2435–2442.
- (58) Tsamaloukas, A. D.; Keller, S.; Heerklotz, H. *Nat. Protoc.* **2007**, *2*, 695–704.
- (59) Rekharsky, M. V.; Mori, T.; Yang, C.; Ko, Y. H.; Selvapalam, N.; Kim, H.; Sobransingh, D.; Kaifer, A. E.; Liu, S.; Isaacs, L.; Chen, W.; Moghaddam, S.; Gilson, M. K.; Kim, K.; Inoue, Y. *Proc. Natl. Acad. Sci. U. S. A.* **2007**, *104*, 20737–20742.
- (60) Israelachvili, J. N.; Mitchell, D. J.; Ninham, B. W. *J. Chem. Soc., Faraday Trans. 2* **1976**, *72*, 1525–1568.
- (61) Lee, O.-S.; Stupp, S. I.; Schatz, G. C. *J. Am. Chem. Soc.* **2011**, *133*, 3677–3683.
- (62) Berendsen, H. J. C.; Postma, J. P. M.; van Gunsteren, W. F.; Hermans, J. *The 14th Jerusalem Symposium on Quantum Chemistry and Biochemistry*, Pullman, B., Ed.; Springer Netherlands: Dordrecht, 1981; pp 331–342.
- (63) Scott, W. R. P.; Hunenberger, P. H.; Tironi, I. G.; Mark, A. E.; Billeter, S. R.; Fennen, J.; Torda, A. E.; Huber, T.; Kruger, P.; van Gunsteren, W. F. *J. Phys. Chem. A* **1999**, *103*, 3596–3607.
- (64) Jain, A.; Ramanathan, V.; Sankaramakrishnan, R. *Protein Sci.* **2009**, *18*, 595–605.